Fluidized-Bed Chemical Vapor Deposition of Silicon on Very Dense Tungsten Powder

Florence Vanni, Mélanie Montaigu, Brigitte Caussat, Carine Ablitzer, Xavière Iltis, Méryl Brothier

DOI: 10.1002/ceat.201400350

Florence Vanni[1]
Mélanie Montaigu[2]
Brigitte Caussat[2]
Carine Ablitzer[1]
Xavière Iltis[1]
Méryl Brothier[1]

[1]CEA Cadarache, DEN/DEC, St-Paul-lez-Durance, France.

[2]University of Toulouse, Laboratoire de Génie Chimique UMR CNRS 5503, ENSIACET/INPT, Toulouse, France.

Fluidized-Bed Chemical Vapor Deposition of Silicon on Very Dense Tungsten Powder

A very dense tungsten powder was coated by silicon from silane using the fluidized-bed chemical vapor deposition process. A reactor of reduced diameter was developed in order to decrease the weight of powders treated. Results show that the fluidization of this powder is possible in this reactor, but with non-optimal gas solid contact induced by the high powder density. Important disturbances of the fluidized-bed temperatures appeared in the presence of silane, due to a partial bed defluidization related to the cohesive nature of the deposit. These disturbances are clearly exacerbated by the exceptional density of the particles. This is probably why a powder agglomeration has been unavoidable when the bed temperature was too low and/or the silane inlet concentration too high. However, a set of operating parameters could be found, allowing a uniform and continuous coating of the whole powder surface.

Keywords: Chemical vapor deposition, Fluidization, Silicon coating, Silane, Very dense powder

1 Introduction

Fluidized-bed chemical vapor deposition (FBCVD) is an efficient process to uniformly coat powders by a great variety of materials [1]. FB reactors have excellent heat and mass transfer capacities, high throughput rates, and can operate continuously, thus reducing operating costs [2, 3]. Silicon from silane (SiH_4) precursor is certainly the most studied coating material using this process because of its development for producing solar-grade silicon to replace the Siemens process [3–11]. It is worth noting that the literature works have most often been conducted on easy-to-fluidize Geldart's group B powders [12], and employing FB reactors of internal diameters between 5 and 20 cm. The particles coated by Si FBCVD from silane are generally silicon seeds for the photovoltaic industry [3–11].

New nuclear fuels with limited enrichment in ^{235}U are under development for research nuclear reactors. Powdered U(Mo) metallic fuels dispersed in an aluminum-base matrix appear among the most promising materials. However, interfacial interactions between the fuel and its matrix can occur under irradiation, leading to a huge swelling of the fuel [13]. A solution could be to coat the fuel powder by a barrier before its dispersion into the matrix. Silicon seems to be a good candidate [14]. Some promising irradiation tests have been performed with U(Mo) coated with Si by physical vapor deposition (PVD) [15, 16]. FBCVD could be another way to provide U(Mo) coated with Si, but its evaluation remains to be done.

Galerie et al. [17] have analyzed the deposition kinetics during silicon FBCVD from silane on iron particles at temperatures lower than 400 °C without giving information on the process. To the best of our knowledge, no other study in literature deals with FBCVD of Si from silane on metallic particles.

The metallic fuel U(Mo) powder has a very high density of about 17 500 kg m^{-3} [18] close to that of tungsten (19 300 kg m^{-3}). This explains why a tungsten powder of mean diameter close to that of the fuel powder has been used to analyze the feasibility to deposit silicon by FBCVD from silane. To the best of our knowledge, this process has never been used to coat such dense powders.

In a previous work of our group, the ability to fluidize this powder has been demonstrated in a reactor of 5 cm internal diameter [19]. However, the application requires minimizing the weight of powder used for each coating experiment. Consequently, in the present study, a FBCVD reactor of reduced diameter (3.8 cm) has been tested.

First, experimental results about the fluidization hydrodynamics of the tungsten powder in this reactor will be presented prior to detail the thermal behavior of the FBCVD process and then the results obtained about silicon deposition from silane.

2 Experimental

The FBCVD reactor for this study consists of a vertical cylindrical column of stainless steel, with 3.8 cm internal diameter and 1 m height. It is externally heated by a two-zone electrical

Correspondence: Prof. Brigitte Caussat (Brigitte.Caussat@ensiacet.fr), Laboratoire de Génie Chimique, ENSIACET/INPT, 4 allée Émile Monso, BP 44362, 31432 Toulouse Cedex, France.

furnace and the wall temperatures are monitored by two thermocouples. Five thermocouples are also bundled into a 6 mm diameter stainless-steel tube, placed inside the reactor in order to measure the bed temperatures at various heights. A sixth thermocouple is placed under the stainless-steel porous plate used for gas distribution. The inlet flow rates of silane (SiH_4; Air Liquide, N50) diluted in argon (Air Liquide, Alpha1) are controlled by a ball rotameter and a mass flow controller, respectively. A differential fast response pressure sensor with taps under the distributor and top of the column measures the total pressure drop across the bed. Moreover, an absolute pressure sensor allows monitoring the total pressure below the distributor. A DasyLab® system enables the online acquisition of differential pressure, total pressure, and axial profile of bed temperatures.

The FBCVD reactor was also used to perform fluidization tests at room temperature and around 600 °C with pure argon as carrier gas. Some fluidization tests at room temperature were also carried out in a glass fluidization column with an internal diameter of 0.05 m and a height of 1 m, equipped with the same porous plate distributor. All experiments were performed under atmospheric pressure.

The tungsten powder was supplied by NEYCO (CERAC, Inc. T-1220). Its grain density is equal to 19 300 kg m^{-3}. The particle size distribution values measured by laser granulometry analysis on a Malvern MasterSizer Sirocco 2000 in dry mode as illustrated in Fig. 1 a indicated that the distribution of the particle diameters D_{10}/D_{90} is 50 µm/105 µm with a Sauter diameter $D_{3,2}$ of 70 µm.

Fluidization hydrodynamics was studied by plotting the bed pressure drop versus increasing and decreasing gas superficial velocity. A normalized bed pressure drop ΔP^* was calculated by dividing the bed pressure drop measured experimentally by the theoretical bed pressure drop, equal to the bed weight per column surface area. A normalized bed expansion H^* was also measured as the ratio between the expanded bed height and the initial fixed bed height.

The morphology of the initial powder and of the coated particles was observed by scanning electron microscopy (SEM; Philips XL 30 FEG and LEO 435 VP). SEM observations highlighted that tungsten particles are non-spherical and faceted, as demonstrated in Fig. 1 b. X-Ray diffraction (XRD) analyses were performed on the compacted powders before and after deposition on a Seifert-3000TT equipment.

3 Results and Discussion

All the results below were obtained without premixing of the powder once placed in the columns. Fig. 2 presents the normalized bed pressure drop curves obtained in the glass column of 5 cm and in the FBCVD reactor of 3.8 cm at ambient temperature, for 1.3 kg of powder. In both curves, a fluidization horizontal plateau is present for ΔP^* close or equal to 1, proving that a complete fluidization of particles was achieved. In the glass column, a small part of powders remained stuck on the walls due to electrostatic effects, which could explain that the plateau is not exactly observed at $\Delta P^* = 1$ and that an hysteresis appears between increasing and decreasing curves.

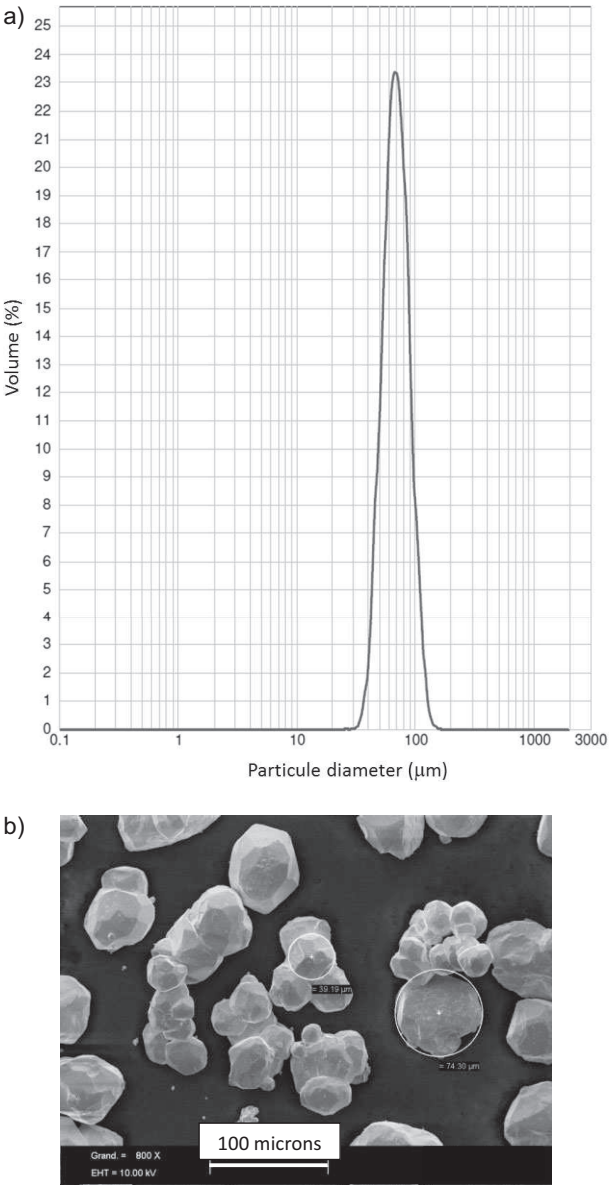

Figure 1. (a) Volume diameter distribution, (b) SEM micrograph of the tungsten powder.

The minimum fluidization velocity U_{mf} was classically determined by the method of Davidson and Harrison [20] at decreasing gas velocity. A similar value of U_{mf} was found in the two reactors, near to 2.7 cm s^{-1}. This value is very close to that previously found in the 5-cm stainless-steel FBCVD reactor using pure argon [21]. According to Liu et al. [22] and to Guo et al. [23], when the reduction of the reactor diameter leads to modifications of the FB hydrodynamics, the U_{mf} value increases and a pressure overshoot appears on the pressure drop curves, due to wall effects. In our case, it can then be concluded that the FB hydrodynamics is not markedly modified by the reactor diameter reduction. Liu et al. found that wall effects only appear for reactors of diameter below 2 cm, called micro FB, which is coherent with our own results, even if the density of the powders is very different.

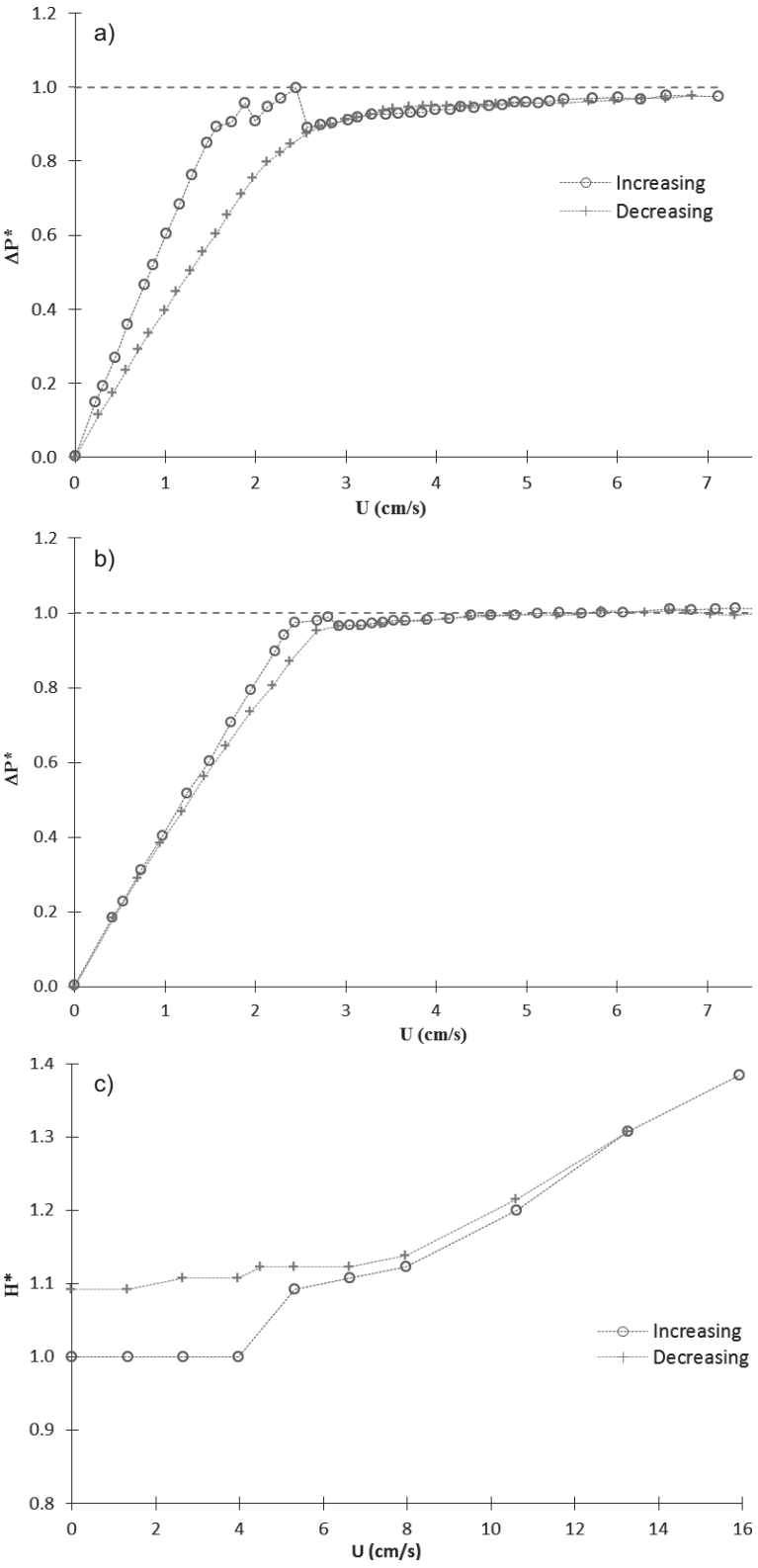

Figure 2. (a) Normalized bed pressure drop in the glass column with 5 cm diameter and (b) in the FBCVD reactor with 3.8 cm diameter, (c) normalized bed expansion in the glass column vs. increasing and decreasing argon velocities at ambient temperature.

The bed expansions generally vary between 1.2 and 2 for conventional fluidized beds [24, 25]. In our case (Fig. 2 c), the bed expansions do not exceed 1.4, even for a fluidization ratio U/U_{mf} of 6. This can be explained by the fact that in a fluidized bed the particles are submitted to three different major forces, the gravitational force, i.e., the weight of particles, the gas-particle interaction drag force, and the particle-particle or particle-wall interaction force. According to Wang et al. [26], when very dense particles are fluidized, the gravitational force dominates the others. As a consequence, the bed expansion is low meaning that the number and size of gas bubbles into the bed are low, too. Even if bubbles can have negative impacts such as gas bypassing through bubbles, it is clear that bubble motion and gas circulation around the bubbles contribute to good gas and solids mixing.

One of the most famous empirical correlations predicting the fluidized-bed expansion, especially for Geldart's group A particles, is that of Richardson and Zaki [27]. This correlation indicates that bed expansion decreases if the particle density increases, meaning that for very dense powders the gas-solid contact is of lower quality. A hysteresis exists between the increasing and decreasing expansion curves at low gas velocity. This means that the powder is aeratable as Geldart's group A particles, probably due to its quite low mean diameter [28]. So, even if non-optimal, the FB hydrodynamics seems convenient to ensure good thermal and mass transfers conditions necessary to perform CVD in this reactor with reduced diameter.

The operating conditions tested by FBCVD and the average bed temperatures before, during, and after each deposition experiment are detailed in Tab. 1. The operating parameters were chosen on the basis of previous results of our group [6, 29], in order to not agglomerate the bed and to form silicon deposits of at least 0.5 µm thickness for an easier characterization. For all runs, the fluidization ratio U/U_{mf} was fixed to 5.3 and the weight of powders was 1.5 kg corresponding to a ratio between the fixed bed height and the reactor diameter of 3.4.

The experimental results are summarized in Tab. 2. The silane conversion rates and weight percentages of silicon deposited on powders were deduced from bed weighing before and after deposition. A theoretical thickness of silicon was also calculated from the mass of deposited silicon on the bed, assuming that the deposit is uniform on the whole powder surface. The real thickness of the coatings was determined from SEM analyses in a cross section after mechanical polishing of embedded powders in epoxy or after crushing the coated particles.

As detailed in Tab. 2, laser size analyses performed after each run indicate that the Sauter

Table 1. Operating conditions tested and measured average bed temperatures.

Run	Silane inlet vol. [%]	Run duration [min]	Average bed *T* before deposition [°C]	Average bed *T* during deposition [°C]	Average bed *T* after deposition [°C]
W2quater	2.6	120	587	597	604
W3	2.6	120	606	608	609
W4	5.2	60	621	624	620
W5[a]	5.2	15	605	621	580
W6	2.6	120	618	625	621
W7 [a)]	4–2.9	60	604	602	603

[a)] These runs have led to irreversible bed agglomeration.

Table 2. Experimental results.

Run	Silane conversion rate [%]	Silicon [wt %] deposited on powders	Thickness deduced from bed weighing [µm]	Thickness deduced from SEM [µm]	Sauter diameter of powders [µm]
W2quater	100	0.83	0.76	0.75	70.9
W3	100	0.96	0.87	0.72	71.3
W4	100	0.78	0.71	0.53	70.9
W5[a)]	–	–	0.27	–	–
W6	100	0.97	0.88	0.8	72.4
W7 [a)]	93.4	0.4	0.37	0.37	69.5

[a)] These runs have led to irreversible bed agglomeration.

diameter of powders is slightly higher than the initial one, indicating that no bed agglomeration occurred, except for runs W5 and W7. The deposit thicknesses could not be deduced from these results because they are in the measurement uncertainty of the method.

Fig. 3 presents the thermal profiles obtained during runs W6, W5, and W7. They are characteristic of the whole thermal profiles obtained without and with bed agglomeration phenomena. The heating step duration was around 70 min. Once stable thermal profiles were obtained, the FB temperature gradient (thermocouples TC1 to TC5) before silane injection was lower than 10 °C. This confirms that the bed of powders was conveniently fluidized at high temperature. The temperature TC6 measured under the distributor was kept below 200 °C in order to not decompose silane before its entrance into the reactor and to not plug the distributor by silicon deposition.

It is worth noting that for experiments without any agglomeration phenomenon like run W6 (Fig. 3 a), as soon as silane is injected into the bed, a thermal gradient systematically appears, the bottom part of the bed being gradually colder. This gradient was on average close to 70 °C and it systematically decreases a few minutes after the end of silane injection, probably due to a partial and reversible defluidization of the bed.

For a deeper analysis of this phenomenon, Tab. 1 provides the average bed temperatures measured before, during, and after silane injection for each run. It appears that the mean temperatures in the presence of silane are always higher than those before silane injection, from 2 °C to 12 °C depending on the conditions tested. This could be due to an overheating of the furnace to meet its target wall temperature when the bed is partly defluidized, since the gas-solid heat transfers are certainly lower. The temperatures corresponding to the period of 15 min after deposition are also often higher than those before silane injection, certainly due to the thermal inertia of the reactor. The bed pressure drop (not shown) was close to the apparent bed weight before silane injection, slightly increased during deposition by 10 mbar on average, and recovered its initial value after deposition. It is well-known that silicon CVD from silane can involve some reversible disturbances of the bed thermal profile and pressure drop due to a partial defluidization of the bed, probably related to the appearance of short-lived agglomerates. Indeed, silicon dangling bonds are probably formed on the surface of each particle during deposition, acting as a glue for the surrounding particles [5, 6].

Fig. 3 b presents the bed thermal profile during run W5, in which an irreversible agglomeration of powders occurred a few minutes after silane injection. A sharp increase of the bed pressure drop (not shown) and a marked thermal gradient of more than 200 °C were rapidly observed along the bed, leading to the immediate stop of silane feeding.

Run W7 began with 4 vol % of silane but since strong disturbances of temperatures and of bed pressure drop rapidly appeared, the silane molar fraction was reduced to 2.9 %, thus leading to more stable process conditions (Fig. 3 c). But the thermal gradient remained higher than for runs performed at lower inlet silane concentration.

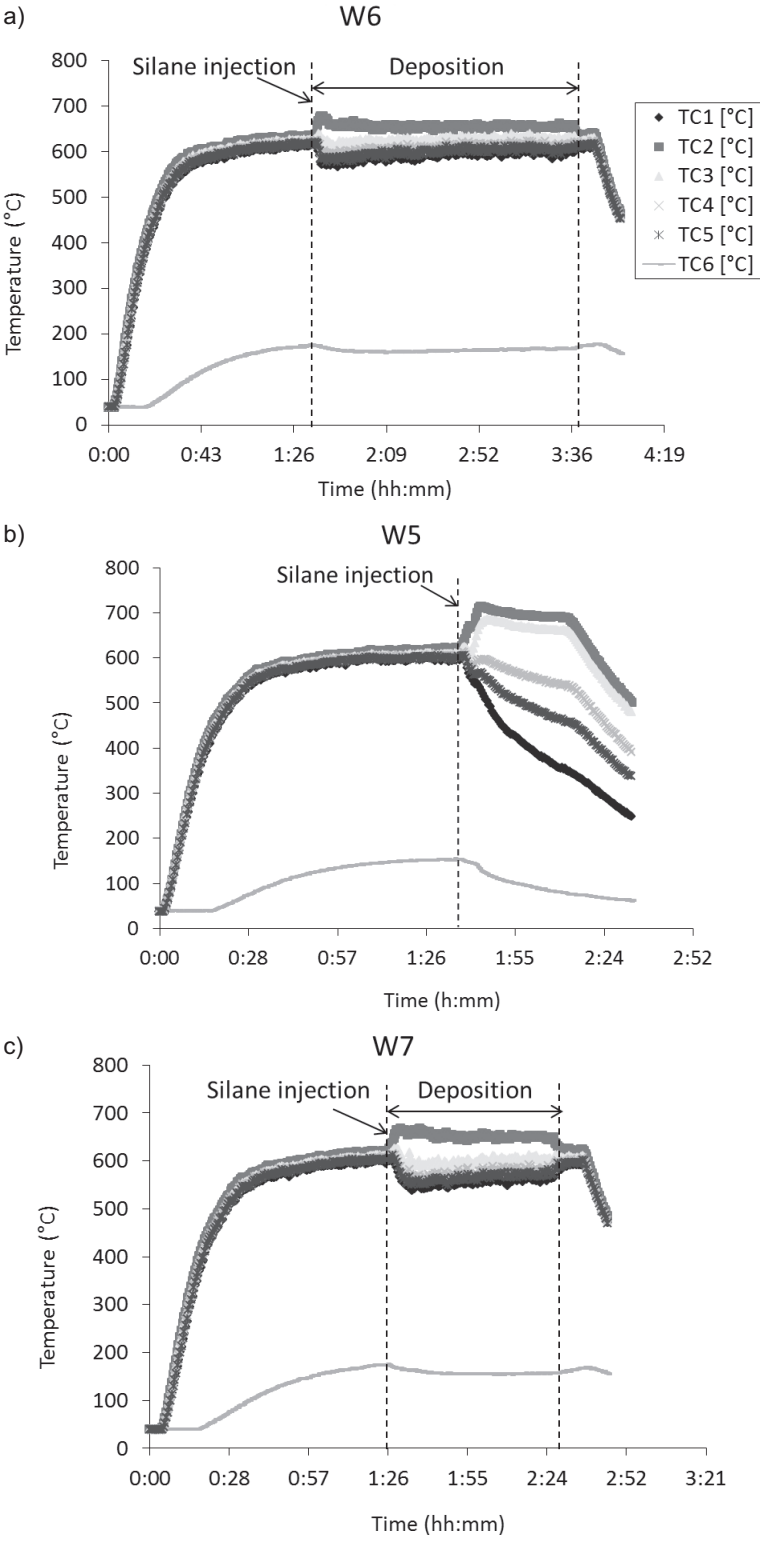

Figure 3. Thermal profiles in the bed (TC1 to TC5) and below the distributor (TC6) during runs (a) W6, (b) W5, (c) W7. Heights above the distributor for thermocouple TC1: 1 cm, TC2: 12 cm, TC3: 7 cm, TC4: 5 cm, TC5: 2.5 cm.

In the case of silicon FBCVD on powders of conventional density, most often of Geldart's group B, and with reactors of larger diameter [3–11], the bed thermal disturbances are clearly lower than in our case even for much higher silane inlet molar fractions. This means that neither the variations of the fluidization gas properties nor the reaction enthalpy can explain the bed pressure drop and thermal profiles disturbances we observed. The latter are clearly linked to the very high density of the tungsten particles.

As previously explained, fluidized particles are submitted to three different major forces, namely, the weight of particles, the gas-particle interaction drag force, and the particle-particle or particle-wall interaction force. Different particle-particle forces can coexist, which are either repulsive like the solid collision forces or attractive like the Van der Waals or the electrostatic forces. In the case of silicon deposition from silane, a specific attractive force appears, related to the deposition chemistry on the particle surface. As long as the repulsive forces are higher than the attractive ones, for worse only a partial defluidization is observed, leading to higher bed pressure drop and thermal profiles. When this is not the case, an irreversible agglomeration of particles occurs. In the case of the very dense tungsten particles, we have previously explained that the dominant force into the bed without silane is the weight of particles, meaning that the repulsive force linked to particle collisions is lower than for powders of more classical density. So, the silane concentrations for which agglomeration happens are lower than for conventional powders.

Agglomeration seems to be exalted if the silane concentration is increased (runs W5 and W7 compared to run W3) and/or if the bed temperature is decreased (run W5 compared to run W4). It is likely that the number of Si dangling bonds per unit surface area of powder increases with silane concentration. The chemistry and kinetics of silane pyrolysis and of silicon deposition are probably slightly different at 600 °C and at 620 °C, leading to more numerous dangling bonds at 600 °C.

As desired, for the runs without agglomeration, the silane conversion rate was always close to 100 % as detailed in Tab. 2. These good conversion rates are due to the combination of low inlet silane concentrations, sufficiently high bed temperatures, and large enough residence times of the reactive gas into the bed [29]. The theoretical thicknesses deduced from bed weighing before and after deposition were always larger than 0.5 µm as initially planned, except for the two peculiar runs W5 and W7.

SEM views of the powder surface before and after silicon deposition are displayed in Fig. 4. The difference between coated and uncoated tungsten surface is obvious: the nontreated surface of particles is relatively smooth, whereas the silicon deposit forms a nodular film. Such morphology is characteristic of silicon CVD films from silane for this range of temperatures under atmospheric pressure [5, 6]. This is due to the fact that sili-

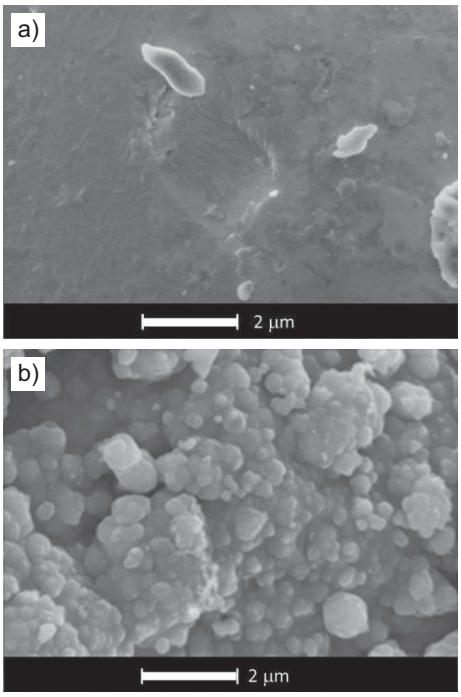

Figure 4. SEM micrographs of the tungsten powder (a) before and (b) after deposition.

con deposition in an FB reactor not only involves heterogeneous deposition mechanisms from silane, but also homogeneous formation of silicon nuclei in the gas phase, which can be scavenged by the bed particles [11]. It is worth noting that for all experiments the top part of the reactor was covered by a very thin brown layer probably formed of these homogeneously born silicon nuclei. No clear trend appears for the influence of bed temperature or of silane inlet concentration on the coating morphology, probably because the ranges of variation are too small.

Fig. 5 presents SEM views of crushed powders after runs W4 and W6, on which the uniformity and continuity of the deposit on the tungsten surface clearly appears as its nodular morphology. On these SEM micrographs, it is not possible to distinguish an intermediate layer between the substrate and the Si layer that could indicate the formation of a silicide layer as reported by Yoon et al. [30] in a study about planar CVD of Si on W at higher temperatures of 1000 °C and more. It is worth noting that the deposit thickness can be estimated on these micrographs. For the whole runs without bed agglomeration, the measured thicknesses are close to those deduced from bed weighing as detailed in Tab. 2, thus proving the uniformity of the deposit over the whole powder surface. This is a major result since it indicates that even if the bed was partly defluidized, the mixing of the powders by the gas was intense enough to ensure uniform deposition conditions.

Some XRD measurements were performed before and after experiments as illustrated in Fig. 6, revealing that for all the conditions tested, the silicon deposit is composed of amorphous and polycrystalline phases, with {111} and {220} preferential orientations. Such mixed product is a classical result for the range of temperatures tested [11]. These crystalline preferential orientations of silicon were also obtained in another

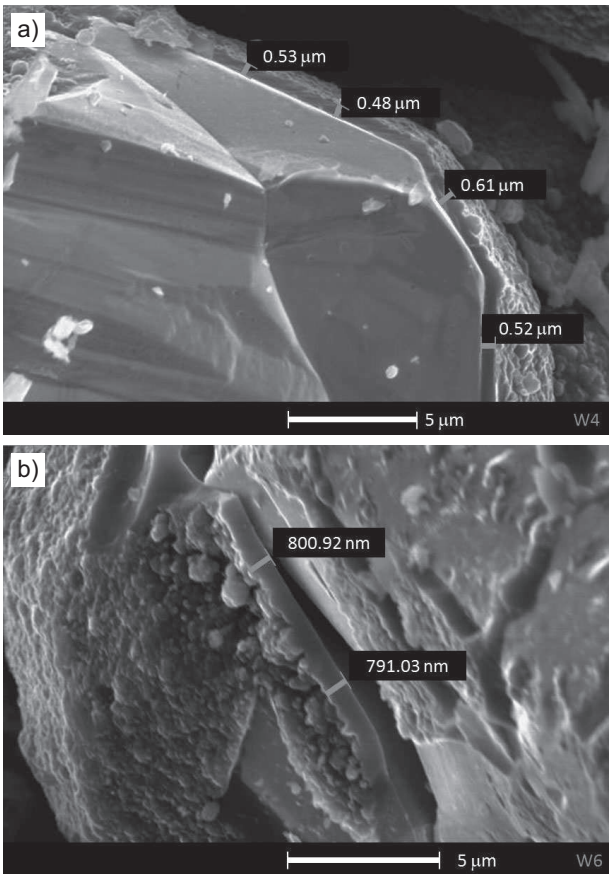

Figure 5. SEM micrographs of some crushed tungsten particles after (a) run W4, (b) run W6.

work on planar substrates in the same range of temperatures [31]. No influence of the temperature appears on the XRD diffractometers, certainly due to the fact that the tested temperature range is quite small.

4 Conclusions

Very dense tungsten powders simulating nuclear fuel particles were coated by silicon from silane (SiH_4) using the fluidized-bed chemical vapor deposition process. A reactor of reduced diameter in comparison with previous works was selected in order to decrease the weight of powder.

First, it could be verified that the decrease of reactor diameter from 5 to 3.8 cm does not modify the fluidization behavior of the tungsten powder. These particles can fluidize with characteristics of Geldart's group A powders due to their small mean diameter, but with non-optimal gas solid contact certainly induced by their exceptional density.

Then, operating conditions involving inlet molar fractions of silane between 2.6 to 5.2 % in argon and bed temperatures between 590 °C and 625 °C were determined, allowing to uniformly deposit continuous silicon films of at least 0.5 µm thickness on the whole surface of the powder. The coatings are of nodular morphology and appear as mixed-phase, amorphous, and polycrystalline.

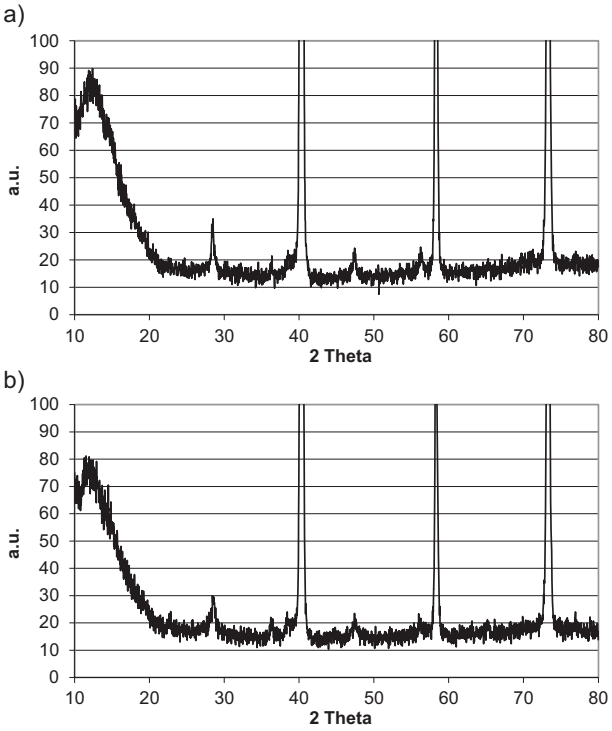

Figure 6. XRD diffractomers of the powder after (a) run W2quater and (b) run W6.

When the inlet molar fraction of silane was too high and/or the bed temperature too low, an irreversible bed agglomeration occurred. Moreover, bed thermal gradients and pressure drop disturbances classically associated to this process were more intense than in previous works involving easy-to-fluidize powders and larger reactor diameters. This could be due mainly to the high density of the tungsten powder and also to the decrease of reactor diameter, both reducing the intensity of the gas-solid mixing and thus favoring defluidization phenomena induced by the cohesive nature of the silicon deposit.

These results prove that the FBCVD process is an appropriate technology to deposit silicon coatings on very dense particles, even in a reactor of reduced diameter. New experiments are in progress in order to study higher deposition temperatures to better meet barrier requirements for nuclear fuel applications.

Acknowledgment

The authors would like to thank Michel Molinier, Etienne Prevot, and Marie Line de Solan from LGC as well as Nicolas Tarisien from CEA for technical support.

The authors have declared no conflict of interest.

References

[1] C. Vahlas, B. Caussat, P. Serp, G. Angelopoulos, *Mater. Sci. Eng. Res.* **2006**, *53*, 1–72.

[2] B. E. Ydstie, J. Ju, in *Solar Cells – Silicon Wafer-Based Technologies* (Ed: L. A. Kosyachenko), InTech Europe, Rijeka, Croatia **2011**, 125–138.

[3] S. S. Liu, W. D. Xiao, *Chem. Eng. Sci.* **2014**, *111*, 112–125.

[4] G. Hsu, N. Rohatgi, J. Houseman, *AIChE J.* **1987**, *33*, 784.

[5] T. Kojima, H. Hiroha, K. Iwata, T. Furusawa, *Int. Chem. Eng.* **1992**, *32*, 739–749.

[6] B. Caussat, M. Hémati, J. P. Couderc, *Chem. Eng. Sci.* **1995**, *50*, 3615–3624.

[7] M. P. Tejero-Ezpeleta, S. Buchholz, L. Mleczko, *Can. J. Chem. Eng.* **2004**, *82*, 520–529.

[8] J. Pina, V. Bucala, P. Ege, H. de Lasa, *Int. J. Chem. Reactor Eng.* **2006**, *4*, 1–21.

[9] S. Balaji, J. Du, C. M. White, B. E. Ydstie, *Powder Technol.* **2010**, *199*, 23–31.

[10] C. J. Wang, T. F. Wang, Z. W. Wang, *Chem. Eng. Technol.* **2012**, *35*, 893–898.

[11] W. O. Filtvedt, A. Holt, P. A. Ramachandran, M. C. Melaaen, *Sol. Energy Mater. Sol. Cells* **2012**, *107*, 188–200.

[12] D. Geldart, *Powder Technol.* **1973**, *7*, 285–292.

[13] A. Leenaers, S. Van den Berghe, E. Koonen, C. Jarousse, F. Huet, M. Trotabas, M. Boyard, S. Guillot, L. Sannen, M. Verwerft, *J. Nucl. Mater.* **2004**, *335*, 39–47.

[14] T. Zweifel, H. Palancher, A. Leenaers, A. Bonnin, V. Honkimaki, R. Tucoulou, S. Van Den Berghe, R. Jungwirth, F. Charollais, W. Petry, *J. Nucl. Mater.* **2013**, *442*, 124–132.

[15] S. Van den Berghe, A. Leenaers, C. Detavernier, *Proc. of Research Reactor Fuel Management (RRFM)*, Marrakech, Marocco **2010**.

[16] S. Van den Berghe, A. Leenaers, C. Detavernier, *Proc. of Research Reactor Fuel Management (RRFM)*, Rome **2011**.

[17] A. Galerie, G. Le Dû, M. Caillet, P. A. Mari, B. Pingaux, *J. Phys.* **1989**, *50*, C5-709–C5-717.

[18] H. J. Ryu, J. M. Park, K. H. Lee, B. O. Yoo, Y. H. Jung, Y. J. Jeong, Y. S. Lee, Y. S. Kim, *RRFM, European Research Reactor Conference*, Saint Petersburg, Russia, April **2013**.

[19] P. Rodriguez, B. Caussat, C. Ablitzer, X. Iltis, M. Brothier, *J. Nanosci. Nanotechnol.* **2011**, *11*, 8083–8088.

[20] J. F. Davidson, D. Harrison, *Fluidised Particles*, Cambridge University Press, New York **1963**.

[21] P. Rodriguez, B. Caussat, C. Ablitzer, X. Iltis, M. Brothier, *Chem. Eng. Res. Des.* **2013**, *91*, 2477–2483.

[22] X. Liu, G. Xu, S. Gao, *Chem. Eng. J.* **2008**, *137*, 302–307.

[23] Q. J. Guo, Y. Xu, X. Yue, *Chem. Eng. Technol.* **2009**, *32*, 1992–1999.

[24] D. C. Saua, S. Mohanty, K. C. Biswal, *Chem. Eng. Proc.* **2010**, *49*, 418–424.

[25] D. Geldart, A. C. Y. Wong, *Chem. Eng. Sci.* **1984**, *39*, 1481–1488.

[26] Y. Wang, Y. Cheng, Y. Jin, H. T. Bi, *Powder Technol.* **2007**, *172*, 167.

[27] J. F. Richardson, W. N. Zaki, *Trans. Inst. Chem. Eng.* **1954**, *32*, 35–53.

[28] A. Castellanos, *Adv. Phys.* **2005**, *54*, 263–376.

[29] L. Cadoret, C. Rossignol, J. Dexpert-Ghys, B. Caussat, *Mater. Sci. Eng. B* **2010**, *170*, 41–50.

[30] J. K. Yoon, K. W. Lee, S. J. Chung, I. J. Shon, J. M. Doh, G. H. Kim, *J. Alloys Comp.* **2006**, *420*, 199–206.

[31] J. M. Westra, V. Vavrunkova, P. Sutta, M. Seman, *Energy Procedia* **2010**, *2*, 235–241.